Physica C 470 (2010) 456–460

Contents lists available at ScienceDirect

Physica C

journal homepage: www.elsevier.com/locate/physc

Comparative study of the core level photoemission of the ZrB_2 and ZrB_{12}

L. Huerta [a], A. Durán [b], R. Falconi [c], M. Flores [d], R. Escamilla [a,*]

[a] Instituto de Investigaciones en Materiales, Universidad Nacional Autónoma de México, 04510 México D.F., Mexico
[b] Centro de Nanociencias y Nanotecnologia, Universidad Nacional Autónoma de México, Apartado Postal 2681, Ensenada, Baja California 22800, Mexico
[c] División Académica de Ciencias Básicas, Universidad Juárez Autónoma de Tabasco, Cunduacán, Tabasco, CP 86690, AP 24, Mexico
[d] Departamento de Ingeniería de Proyectos, CUCEI, Universidad de Guadalajara, AP 307, Zapopan Jal 45101, Mexico

ARTICLE INFO

Article history:
Received 19 October 2009
Received in revised form 9 March 2010
Accepted 22 March 2010
Available online 27 March 2010

Keywords:
Zirconium diboride
Zirconium dodecaboride
Band structure
XPS
UPS
DOS

ABSTRACT

X-ray photoelectron spectroscopy (XPS) and ultraviolet photoelectron spectroscopy (UPS) were used to investigate the binding energies and valence band for ZrB_2 and ZrB_{12}. The Zr 3*d* and B 1*s* core levels were identified. The Zr 3*d* core level shows a spin–orbit split $3d_{5/2}$ and $3d_{3/2}$ while that for B 1*s* core level exhibited a single symmetric peak, these being typical of zirconium and boride signals. Comparing the Zr 3*d* and B 1*s* core levels with metallic Zr, B_2O_3 and ZrO_2 reference materials only a negative chemical shift for Zr 3*d* associated to ZrB_2 was observed, which suggests that the charge transfer model based on the concept of electronegativity was not applicable to explain the superconductivity in the ZrB_{12} sample. The measured valence band using UPS is consistent with the band-structure calculations indicating a higher density of states (DOS) at E_F for ZrB_{12} respect to ZrB_2. Finally, we found that the weak mixed B-*p* and Zr-*d* states for ZrB_{12} is crucial for the superconductivity due to the state population increased the DOS at the E_F.

1. Introduction

The discovery of superconductivity in MgB_2 at about 40 K by Nagamatsu et al. [1] generated a great deal of excitement and many studies related to both fundamental and practical aspects. Many researchers have investigated other boron containing phases, for example: borides, diborides, hexaborides and dodecaborides. For these phases, the Zr based ones are interesting because some are superconductors but not all are isostructural to the MgB_2. ZrB_2 crystallizes in a simple hexagonal AlB-type structure (S.G. P6/mmm) consisting of two-dimensional graphite-like monolayers intercalated with Zr monolayers [2]. In contrast ZrB_{12} shows a cubic crystalline structure (S.G. Fm-3m), where the Zr atoms and cub-octahedral B_{12}-clusters are arranged as in the NaCl-like structure [3].

ZrB_{12} is found to have the highest superconductivity critical temperature ($T_c \sim 6$ K) in the family of the dodecaborides [3,4]. On the other hand, stoichiometric ZrB_2 is not a superconductor; however recent studies have speculated that the off-stoichiometric compound may be a superconductor at about 5.5 K. The mechanism may be similar to that observed in other diborides compound such as $NbB_{2.5}$, $MoB_{2.5}$ and others [5–7]. To explain the presence and absence of the superconductivity in the binary intermetallic compound some efforts have been made by measuring the transport and spectroscopy properties [8–11].

Although the electronic properties of transition metal diborides and dodecaborides have been well studied; details of the electronic structure for ZrB_2 and ZrB_{12} compounds are not yet completely clear. In this context it is interesting to probe the theoretical predictions by performing systematic XPS and UPS experimental studies in order to understand the role of the chemical state via binding energy core level, and the valence band on the electronic properties of these compounds.

2. Experimental

We synthesized ZrB_{12} polycrystalline samples by the solid-state reaction method. The precursors, commercially available ZrB_2 powder (Aldrich, −325 mesh) and boron (99.5% powder, crystalline, <57 mesh, 99.5 mass%) were mixed in stoichiometric amounts and pressed into pellets 13 mm in diameter and 0.4 g in weight. The pellets were placed on a copper hearth in an arc-melting furnace in high purity argon (99.999%) atmosphere. Phase identification of the samples was done by X-ray diffraction (XRD) Siemens D5000 using Cu Kα radiation and a Ni filter. The intensities were measured in steps of 0.02° for 14 s in the 2θ range 10–110° at room temperature. The lattice parameters were refined using the Rietvelt program based on the least-squares method [12].

The electrical resistance measurements as a function of temperature were made on mechanically compacted powder samples

* Corresponding author.
E-mail address: rauleg@servidor.unam.mx (R. Escamilla).

0921-4534/$ - see front matter © 2010 Elsevier B.V. All rights reserved.
doi:10.1016/j.physc.2010.03.010

using the four probe method. Four gold wires of 10 μm diameter were used for the *R*–*T* measurements. The experiments were performed from room temperature to about 1.6 K.

The electronic structure and chemical analysis was obtained using X-ray photoelectron spectroscopy (XPS). The analysis was carried out using a VG Microtech ESCA2000 Multilab UHV system, with an Mg Kα X-ray source ($h\nu$ = 1253.6 eV), operated at 15 kV and 20 mA beam, and a CLAM4 MCD analyzer. The surface of the pellets was etched for 20 min with 4.5 kV Ar^+ at 0.33 μA mm^{-2}. The XPS spectrum was obtained at 55° to the normal surface in the constant pass energy mode (CAE), E_0 = 50 and 20 eV for survey and high resolution narrow scan, respectively. The peak positions were referenced to the background silver $3d_{5/2}$ photopeak at 368.21 eV, having a FWHM of 1.00 eV, and C 1*s* hydrocarbon groups in 284.50 eV central peak position. The XPS spectra were fitted with the program SDP v 4.1 [13]. The ultraviolet photoelectron spectroscopy (UPS) measurements were performed with a CAE 2.5 eV, using He I ($h\nu$ = 21.2 eV) resonance lines. The XPS error was based on a detection limit estimated to be 0.1% and uncertain propagation. For the deconvolution analysis the uncertain estimated was 5%.

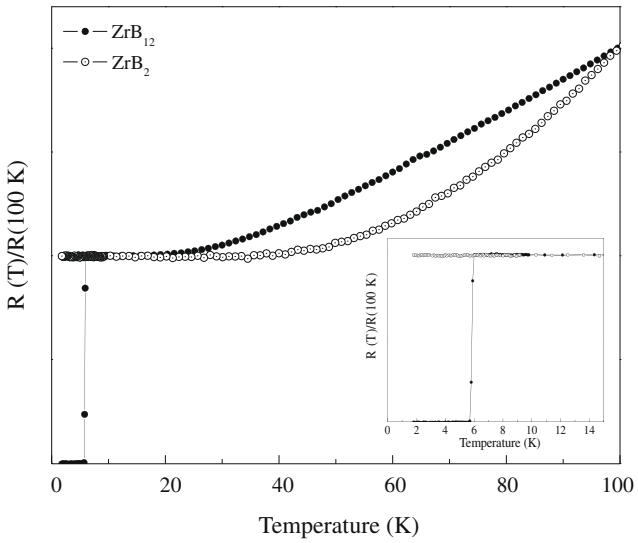

Fig. 2. Normalized resistance as a function of temperature for ZrB_{12} and ZrB_2. Inset: expanded scale at low temperature indicating the superconductivity and non-superconductivity behavior for both intermetallic compound.

3. Results and discussion

Fig. 1 shows the X-ray diffraction patterns for ZrB_{12} and ZrB_2 polycrystalline samples. All characteristics reflections were obtained. The calculated lattice parameter for ZrB_{12} with a cubic structure and space group Fm-3m (No. 225) was a = 7.4102(2) Å; while that for ZrB_2 with a hexagonal structure and space group P6/mmm (No. 191) were a = 3.1652(2) Å and c = 3.5242(2) Å. The lattice parameters are in good agreement with previous works [3,14]. In the dodecaboride, the XRD pattern showed faint features of carbon (ICDD No. 75-1621) associated with impurities as result of the synthesis process.

Fig. 2 shows the normalized resistance as a function of temperature for ZrB_{12} and ZrB_2, respectively. In the range of the temperature measured, T_c with R = 0 is observed at 5.7 K for ZrB_{12}. A sharp transition can be seen with a width (ΔT_c) of 0.2 K indicative of strong intergranular coupling and the absence of the other spurious pair breaking second phases as impurities. On the other hand, the ZrB_2 does not show superconductivity down to 2 K. For clarity, in the inset of Fig. 2 shows an expanded scale of resistivity behavior at low temperature for both compounds. This is in agreement with the results obtained by Leyarovska and Leyarovski [14], according to which no critical transition occurs down to T < 0.7 K. Shein et al. [15] associated the absence of superconductivity to the localization of the Fermi level in the pseudogap between the bonding and antibonding states [16,17]. In relation to this their respective XPS and UPS valence band spectra are discussed later.

In order to understand the role of chemical state via binding energy core level, we analyzed the ZrB_2 and ZrB_{12} by XPS. Fig. 3 shows the XPS survey spectra after Ar^+ etching for 20 min the polycrystalline samples. It was observed that the intensity of the B 1*s* core level corresponding to the ZrB_{12} was higher than that associated to the ZrB_2. On the contrary, the Zr 3*p* and Zr 3*d* core-levels signal associated to the ZrB_2 was more intense than that of ZrB_{12}. Additionally, traces of Ar 2*p*, O 1*s* and C 1*s* were seen in the survey XPS spectra even after repeated sputtering with Ar + of 4.5 kV. Generally, in granular samples, a small peak of C 1*s* was commonly seen in arc-melted samples as a consequence of the initial plasma and the condensation of carbon from vapor oil-combustion and mixing with the re-melted samples.

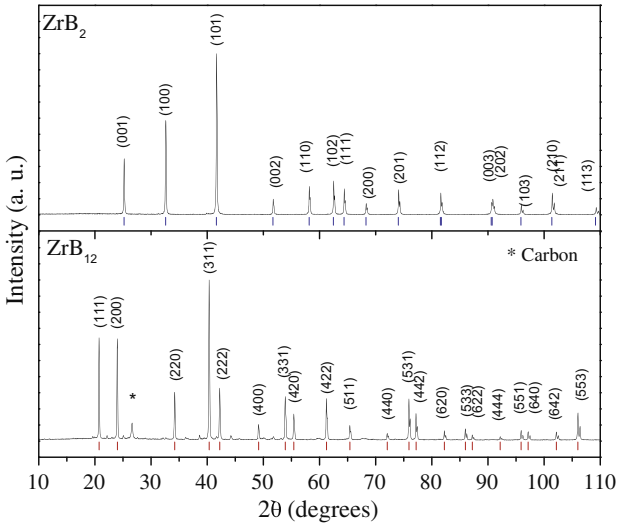

Fig. 1. X-ray diffraction patterns for ZrB_2 and ZrB_{12} samples. (*) indicate carbon.

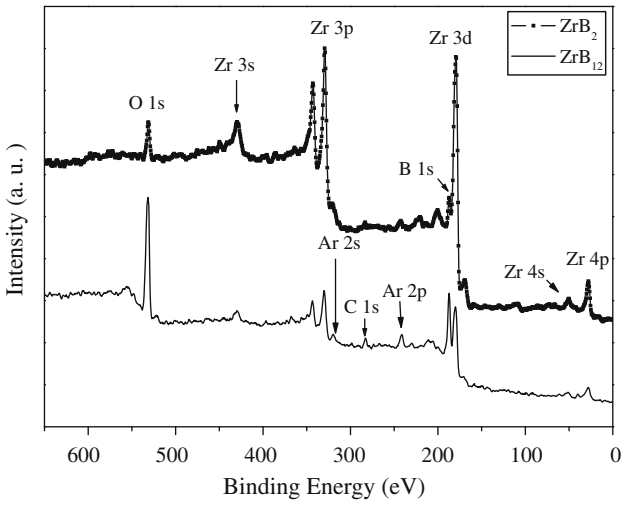

Fig. 3. XPS survey spectra after Ar^+ etching for ZrB_{12} and ZrB_2.

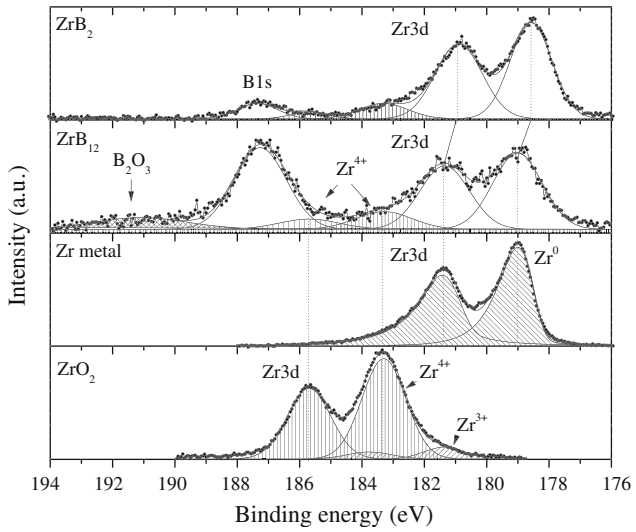

Fig. 4. High resolution XPS spectra of the B 1*s* and Zr 3*d* core-levels for the ZrB_2 and ZrB_{12}. As a reference are used Zr metallic and ZrO_2.

Fig. 4 shows the high resolution XPS spectra of B 1*s* and Zr 3*d* core-levels for ZrB_2 and ZrB_{12} along with metal Zr and zirconia (ZrO_2) as comparative references. The former core level consisted of a single peak while that the latter consisted of the spin–orbit split $3d_{5/2}$ and $3d_{3/2}$. For ZrB_2, the B 1*s* and Zr 3*d* core-levels were localized at a binding energy (BE) of 187.36, 178.58 and 180.85 eV whereas for ZrB_{12} were localized at BE of 187.25, 179.04 and 181.38 eV. The increase of the intensity in B 1*s* core level in ZrB_{12} respect to ZrB_2 was due to high stoichiometric ratio (cuboctahedral B_{12}-cluster framework). Additionally, in ZrB_{12} others peaks of low intensity were observed associated with B_2O_3 and ZrO_2 localized at BE of 191.10, 185.73 and 183.30 eV; the first corresponds to B 1*s* while the others to Zr $3d_{3/2}$ and Zr $3d_{5/2}$. On the other hand, in ZrB_2 two peaks of low intensity were observed associated with Zr 3*d* with BE of 185.70 and 183.30 eV. These ZrO_2 and B_2O_3 traces were not observed in the X-ray diffraction patterns.

The B 1*s* values obtained in this work were in agreement with the reported in typical transition metal diborides [18] and borocarbides RNi_2B_2C (R = Y and La) [19] (187.1–188.3 eV). This observation is consistent with reported calculations and maximum entropy method (MEM) results, which have shown that B–B bonding is two dimensionally covalent (sp^2) [20–22]. Similarly, the Zr 3*d* core level for ZrB_2 are in agreement with the reported by Singh et al. [23]. Note that the corresponding $3d_{5/2}$ and $3d_{3/2}$ core levels for ZrB_{12} are localized in the same BE of metallic Zr.

It is important to point out that the chemical shifts in BE are often used to study the electronic redistribution or charge transfer upon compounds and alloys. In a XPS interpretation, the general rule is that the BE of the central atom increases as the electronegativity of the attached atoms or groups increases [24]. Since B (2.04) is more electronegative than Zr (1.33) according to Pauling's electronegativity table [25], one would expect that the B core level shifts toward lower binding energy. As has been observed for MgB_2; the BE of B 1*s* was lower than in pure boron (positive chemical shift) and the BE of Mg 2*p* is higher that Mg metal (negative chemical shift), suggesting that some charge transfer occurs from the magnesium atoms to the boron atoms. This charge transference was induced from σ to π-band which couples with B E_{2g} vibration mode phonons. This is the mechanism of superconductivity which is favored by the above mentioned charge transfer [26–28]. Studies of the valence-electron distribution in MgB_2 by synchrotron X-ray and precision electron-diffraction techniques and first principles calculations confirmed this observation [29]. In order to confirm whether this mechanism takes place in the compound under study, Table 1 shows the B 1*s*, Zr $3d_{5/2}$ peaks position and chemical shift (ΔB 1*s*, ΔZr $3d_{5/2}$) for ZrB_2 and ZrB_{12} as well as peak positions of the referenced materials. Here it can be observed that the general rule based on the electronegativity fails to explain the positive chemical shift of the B 1*s* core level measured in this work, only a negative chemical shift in the Zr $3d_{5/2}$ of ZrB_2 was observed. This fact suggests that the σ band is completely filled in ZrB_2 and confirms that the presence of superconductivity can be not explained only by charge transfer model based on chemical shift effects. The general rule based on the electronegativity fails also in interpreted the superconductivity in the NbB_{2+x} system [30].

In order to compare the electronic structure of ZrB_2 and ZrB_{12} we studied the UPS and XPS valence band spectra. In the upper panel of Fig. 5 we show the UPS and XPS valence band spectra for the compounds under study. With the purpose of a better interpretation of the spectroscopy data, the valence band of ZrB_2 and ZrB_{12} are compared with the theoretical density of states (DOS) as reported in [15,31].

A good correspondence between the XPS and UPS valence band spectra with DOS can be observed. The characteristic features of the UPS valence band spectrum for ZrB_2 show three main regions, one which lies from the Fermi level to ∼−6.0, another from ∼−6.0 to ∼−7.5 and the last from ∼−7.5 to ∼−11.0 eV, respectively. In contrast, the spectrum for ZrB_{12} is divided in two main parts, from the Fermi level to ∼−6.5 and from ∼−6.5 to ∼−11.0 eV, respectively. According to the theoretical DOS data, for ZrB_2 the lowest group centered at the BE of −10 eV comes from the bonding state of B 2*s* orbital, the broad peak from −5.0 to −7.5 eV are predominantly bonding states of the B $2p\sigma$ and $2p\pi$ orbitals in analogy of band structure of MgB_2 [15], whereas the region around of the Fermi levels arises predominantly from a large contribution from the Zr 4*d* orbitals. Respect to ZrB_{12}, the B 2*s* character is predominant at energies of about −15 eV. The σ bonds between the boron atoms form node-less symmetric orbitals within dodecahedral $B1_2$ units. At about −6.5 to −11.0 eV the B 2*s* and B 2*p* contributions are almost identical and at higher energies the ratio between B 2*s* and B 2*p* character decreases steadily.

The σ and π-bonds are distributed from ∼−10 eV to the Fermi level. From −10 to −7 eV the σ-bond occurs whereas the π-bond is distributed mainly from −7 eV to the Fermi level. These bond states are, of course, also involved in bonding between B atoms of the same B_{12} unit and with e_g or t_{2g} states of neighbouring Zr atoms [32].

The different experimental profile in the XPS–UPS and the theoretical DOS spectrum for the ZrB_2 with respect to ZrB_{12} is evidence of the different participation of the −*s*, −*p* and −*d* states in the crystals, which depend of type of crystal packing. As is seen here, the different lattice type (Hex. P6/mmm for ZrB_2 and cubic Fm-3m for ZrB_{12}) affect both the profile of the UPS valence band and the total theoretical DOS but only slightly the common features at the Fermi level edge (see Fig. 5).

Table 1
B 1*s*, Zr $3d_{5/2}$ peaks position and chemical shift (ΔB 1*s*, ΔZr $3d_{5/2}$) for ZrB_2 and ZrB_{12} respect to materials references.

Samples	B 1*s* (eV)	ΔB 1*s* (eV)	Zr $3d_{5/2}$ (eV)	ΔZr $3d_{5/2}$ (eV)
ZrB_2	187.36	0.06	178.58	−0.42
ZrB_{12}	187.25	−0.05	179.04	0.04
Zr			179.00	
ZrO_2			183.30	
B	187.30			
B_2O_3	191.10			

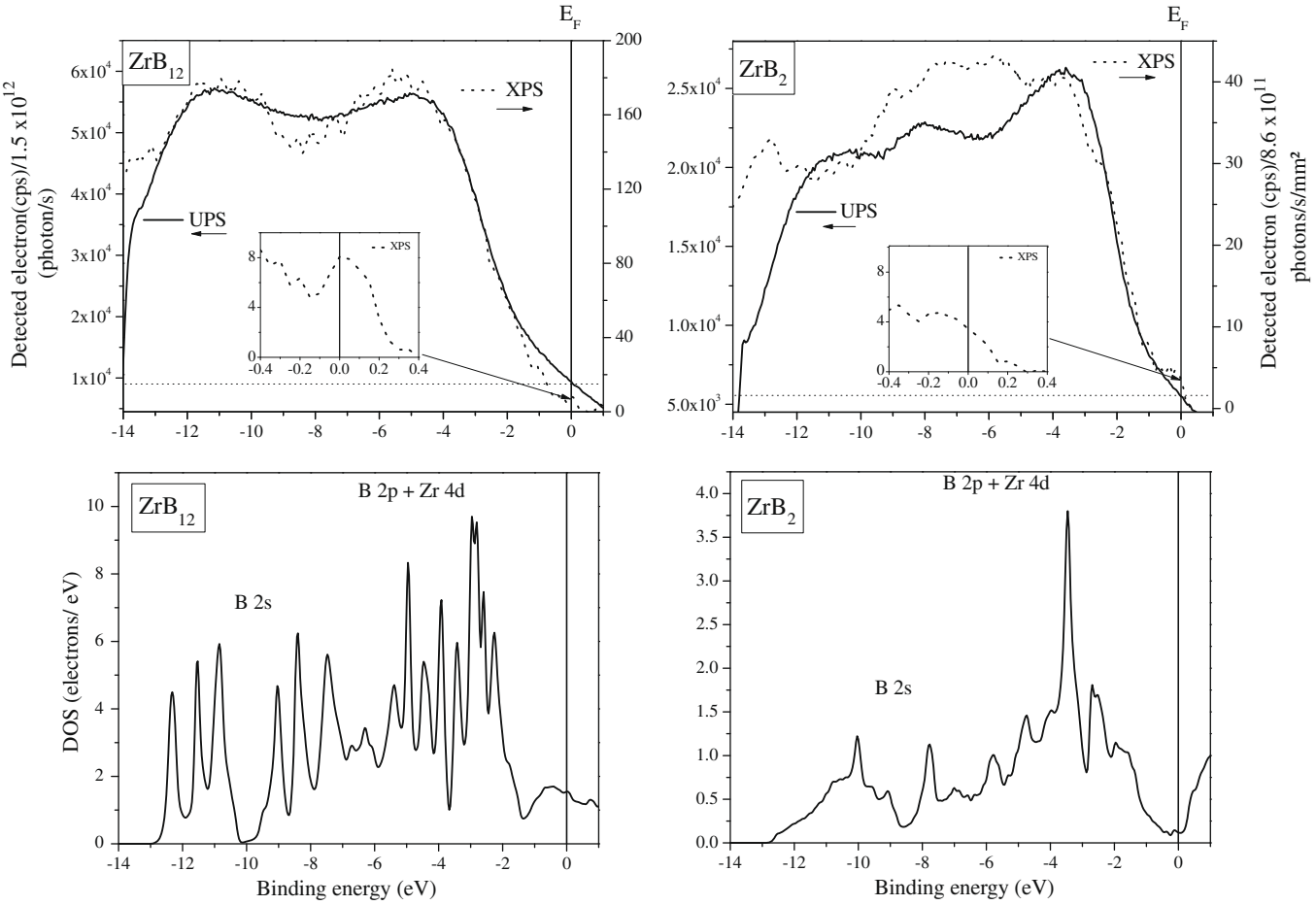

Fig. 5. Comparison of the UPS and XPS valence band spectra of ZrB_2 and ZrB_{12} with the respective density of states (DOS) [16]. Inset shows the expanded scale at the Fermi level.

Comparing the density of states at the Fermi level $N(E_F)$ of ZrB_{12} (1.687 eV^{-1} cell) with ZrB_2 (0.163 eV^{-1} cell) and MgB_2 (0.719 eV^{-1} cell). The lowest density of states at the Fermi level $N(E_F)$ is observed for ZrB_2 in which the Fermi level is located in a depression of DOS between the bonding and antibonding states [33]. In contrast, in the ZrB_{12} the Fermi level is located in a crest and is superconductor (see inset XPS spectra Fig. 5). Similar results were observed in the PrM_2B_2C (M = Ni, Co and Pt) borocarbides, for non-superconductors ($PrNi_2B_2C$ and $PrCo_2B_2C$) the Fermi energy falls in a depression of DOS whereas for the superconductor $PrPt_2B_2C$ borocarbide a peak was seen in the total DOS at the E_F [34]. Thus we believe that the depopulation of the B-*p* state at the Fermi energy gives the lack of superconductivity for ZrB_2. This observation is in agreement with the results obtained by Leyarovska and Leyarovski [14], according to which no critical transition in ZrB_2 occurs down to $T < 0.7$ K.

It is known that the ZrB_{12} is classical Bardeen–Cooper–Schrieffer system with the electron–phonon mechanism of superconductivity [35]. For this system, the important parameter responsible for the formation of their superconducting properties is the orbital composition of the density of states $N(E_F)$ [36]. Comparing the critical temperature T_c of ZrB_{12} with the YB_{12}, it is observed an increase in T_c from 4.7 (YB_{12}) to 5.8 K (ZrB_{12}), which is likely due to an increase in the contribution of the Me 4*d* states to the density of states $N(E_F)$ from 0.532 (YB_{12}) to 0.743 1/eV cell (ZrB_{12}) [15]. However, comparing ZrB_{12} with MgB_2 (T_c = 40 K), the superconducting transition temperature T_c is not simply correlated to the density of states at E_F. Thus we believe that the weak mixed of B-*p* and Zr-*d* states for ZrB_{12} is crucial for the superconductivity since the increase in the DOS at the EF is due to the state's population [17].

4. Conclusions

We have prepared ZrB_{12} by arc-melting method from commercially available ZrB_2 powder precursors. X-ray diffraction pattern showed that the samples were essentially single phase. The XPS studies showed that the stoichiometry of ZrB_{12} and ZrB_2 was stable during large periods of Ar^+ etching time. The deconvolution analysis for ZrB_2 showed that the Zr $3d_{5/2}$ and B 1*s* core levels were localized at 187.36 eV and 178.58 eV, respectively. The respective core levels associated to ZrB_{12} were localized at 187.25 eV and 179.04 eV. Comparing our results with the core levels of the reference materials we observed only a negative chemical shift Zr $3d_{5/2}$ in ZrB_2 indicating that charge transfer does not take place for ZrB_2 and ZB_{12}. The study of the XPS and UPS valence bands for the ZrB_2 and ZrB_{12} phase was consistent with band-structure calculations. Finally, the difference in experimental UPS profiles and the theoretical DOS spectrum of the ZrB_2 and ZrB_{12} was due to the different participation of the *s*, *p* and *d* states in the DOS. In particular, we found that the weak mixed of B-*p* and Zr-*d* states for ZrB_{12} was crucial for the superconductivity since the increase in the DOS at the E_F was due to the state's population.

Acknowledgements

The authors thanks to the projects CONACyT (Nos. 90562), DGAPA-UNAM (Nos. IN227208 and IN112909). For their technical help to G.A. Lara (IIM), F. Silvar (IIM) and J.C. Pineda (IFUNAM).

References

[1] J. Nagamatsu, N. Nakagawa, T. Muranaka, Y. Zenitani, J. Akimitsu, Nature 410 (2001) 63.
[2] E.M. Savitskii, V.V. Baron, Y.V. Efimov, M.I. Bychkova, L.F. Myzenkova, Superconducting Mater., Plenum, New York, 1973.
[3] B.T. Matthias, T.H. Geballe, K. Andres, E. Corenzwit, G.W. Hull, J.P. Maita, Science 159 (1968) 530.
[4] R. Lortz, Y. Wang, S. Abe, C. Meingast, Y.B. Paderno, V. Filippov, A. Junod, Phys. Rev. B 72 (2005) 024547.
[5] V.A. Gasparov, N.S. Sidorov, I.I. Zver'kova, M.P. Kulakov, JETP Lett. 73 (2001) 532.
[6] R. Escamilla, O. Lovera, T. Akachi, A. Duran, R. Falconi, F. Morales, R.J. Escudero, Phys.: Condens. Matter. 16 (2004) 5979.
[7] A.S. Cooper, E. Corenzwit, L.D. Longinotti, B.T. Matthias, W.H. Zachariasen, Proc. Nat. Acad. Sci. 67 (1970) 313.
[8] M.I. Tsindlekht, G.I. Leviev, I. Asulin, A. Sharoni, O. Millo, I. Felner, Y.B. Paderno, V.B. Filippov, M.A. Belogolovskii, Phys. Rev. B 69 (2004) 212508.
[9] R. Khasanov, D.D. Castro, M. Belogolovskii, Y. Paderno, V. Filipov, R. Brutsch, H. Keller, Phys. Rev. B 72 (2005) 224509.
[10] V.A. Gasparov, M.P. Kulakov, N.S. Sidorov, I.I. Zver'kova, V.B. Filipov, A.B. Lyashenko, B. Paderno Yu, JETP Lett. 80 (2004) 330.
[11] H. Ihara, M. Hirabayashi, H. Nakagawa, Phys. Rev. B 16 (1977) 726.
[12] B.A. Hunter, Rietica IUCR Powder Diff. 22 (1997) 21.
[13] SDP v4.1 Copyright© 2004, XPS International, LLC, Compiled 17 January 2004.
[14] L. Leyarovska, E. Leyarovski, J. Less-Common. Met. 67 (1979) 249.
[15] I.R. Shein, A.L. Ivanovski, Phys. Solid State 45 (2003) 1429.
[16] G. Mavel, J. Escard, P. Costa, Castaing J. Surf. Sci. 35 (1973) 109.
[17] K.H. Bennemann, J.B. Ketterson, Conventional and Unconventional Superconductors, Springer-Verlag, Berlin, Heidelberg, 2008.
[18] C.L. Perkins, R. Singh, M. Trenary, T. Tanaka, Y. Paderno, Surf. Sci. 470 (2001) 215.
[19] K. Kobayashi, T. Mizokawa, K. Mamiya, A. Sekiyama, A. Fujimori, H. Takagi, H. Eisaki, S. Uchida, R.J. Cava, J.J. Krajewski, W.F. Peck Jr., Phys. Rev. B 54 (1996) 507.
[20] J.M. An, W.E. Pickett, Phys. Rev. Lett. 86 (2001) 4366.
[21] N.I. Medvedeva, A.L. Ivanovskii, J.E. Medvedeva, A. Freeman, J. Phys. Rev. B 64 (2001) 020502.
[22] E. Nishibori, M. Takata, M. Sakata, H. Tanaka, T. Muranaka, J. Akimitsu, J. Phys. Soc. Jpn. 70 (2001) 2252.
[23] R. Singh, M. Trenary, Y. Paderno, Surf. Sci. Spectra 7 (2000) 310.
[24] W.F. Egelhoff Jr., Surf. Sci. Rep. 6 (1987) 253.
[25] L. Pauling, The Nature of the Chemical Bond, third ed., Cornell University Press, Ithaca, NY, 1957.
[26] I.I. Mazin, O.K. Andersen, O. Jepsen, O.V. Dolgov, J. Kortus, A.A. Golubov, A.B. Kuzmenko, D. van der Marel, Phys. Rev. Lett. 89 (2002) 107002.
[27] R.P. Vasquez, C.U. Jung, M.-S. Park, H.-J. Kim, J.Y. Kim, S.-I. Lee, Phys. Rev. B 64 (2001) 052510.
[28] K.B. Garg, T. Chatterji, S. Dalela, M. Heinonnen, J. Leiro, B. Dalela, R.K. Singhal, Solid State Commun. 131 (2004) 343.
[29] L. Wu, Y. Zhu, T. Vogt, H. Su, J.W. Davenport, J. Tafto, Phys. Rev. B 69 (2004) 064501.
[30] R. Escamilla, L. Huerta, Supercond. Sci. Technol. 19 (2006) 623.
[31] J. Nakamura, N. Yamada, K. Kuroki, T.A. Callcott, D.L. Ederer, J.D. Denlinger, R.C.C. Perera, Phys. Rev. B 64 (2001) 174504.
[32] B. Jäger, S. Paluch, O.J. Żogał, W. Wolf, P. Herzig, V.B. Filippov, N. Shitsevalova, Y. Paderno, J. Phys.: Condens. Matter. 18 (2006) 2525.
[33] C. Jariwala, A. Chainani, S. Tsuda, T. Yokoya, S. Shin, Y. Takano, K. Togano, S. Otani, H. Kito, Phys. Rev. B 68 (2003) 174506.
[34] H. Galvan Donald, A. Durán, A. Posada Amarillas, R. Escudero, Phys. Rev. B 74 (2006) 245121.
[35] C. Buzea, T. Yamashita, Supercond. Sci. Technol. 14 (2001) R115.
[36] S.V. Vonsovskiĭ, Yu.A. Izyumov, É.Z. Kurmaev, Superconductivity of Transition Metals, Their Alloys, and Compounds, Nauka, Moscow, 1977.